



# Nanospectroscopy of thiocyanine dye molecules adsorbed on silver nanoparticle clusters

Uroš Ralević<sup>a</sup>, Goran Isić<sup>a,\*</sup>, Dragana Vasić Anicijević<sup>b</sup>, Bojana Laban<sup>c</sup>, Una Bogdanović<sup>b</sup>, Vladimir M. Lazović<sup>d</sup>, Vesna Vodnik<sup>b</sup>, Radoš Gajić<sup>a</sup>

<sup>a</sup> Graphene Laboratory of Center for Solid State Physics and New Materials, Institute of Physics, University of Belgrade, Pregrevica 118, 11080 Belgrade, Serbia

<sup>b</sup> Vinča Institute of Nuclear Sciences, University of Belgrade, P.O. Box 522, Belgrade, Serbia

<sup>c</sup> Faculty of Natural Sciences and Mathematics, University of Priština, 38200 Kosovska Mitrovica, Serbia

<sup>d</sup> Institute of Physics, University of Belgrade, Pregrevica 118, 11080 Belgrade, Serbia

## ARTICLE INFO

### Article history:

Received 29 June 2017

Received in revised form 13 October 2017

Accepted 21 October 2017

Available online 25 October 2017

### Keywords:

Surface enhanced Raman scattering

Atomic force microscopy

Citrate capped silver nanoparticles

Thiocyanine dye

## ABSTRACT

The adsorption of thiocyanine dye molecules on citrate-stabilized silver nanoparticle clusters drop-cast onto freshly cleaved mica or highly oriented pyrolytic graphite surfaces is examined using colocalized surface-enhanced Raman spectroscopy and atomic force microscopy. The incidence of dye Raman signatures in photoluminescence hotspots identified around nanoparticle clusters is considered for both citrate- and borate-capped silver nanoparticles and found to be substantially lower in the former case, suggesting that the citrate anions impede the efficient dye adsorption. Rigorous numerical simulations of light scattering on random nanoparticle clusters are used for estimating the electromagnetic enhancement and elucidating the hotspot formation mechanism. The majority of the enhanced Raman signal, estimated to be more than 90%, is found to originate from the nanogaps between adjacent nanoparticles in the cluster, regardless of the cluster size and geometry.

© 2017 Elsevier B.V. All rights reserved.

## 1. Introduction

Dye coated metallic nanoparticles (NPs) exhibit interesting optical properties provided by the interaction between the metal core and dye shell. Depending on the interaction mechanism between the two, the optical properties of dye molecules and NPs can be changed separately or jointly within the adsorbate–NP complex [1]. For example, the NP surface plasmon frequency can be changed by the presence of adsorbate while the dye fluorescence can be quenched or enhanced by the NP [2,3]. Ultimately, under special conditions, these complexes can exhibit unique characteristics different than those of either isolated dye molecules or NPs. Owing to the variety of mechanisms by which dyes can interact with metallic NPs, dye–NP complexes can lead to applications ranging from nanoscale sensing [4] to advanced composite materials for novel active and nonlinear optical devices [5].

Many of the recent studies have been focused on dyes which are able to self-assemble in highly oriented structures called J-aggregates on the surface of the NPs [6–14]. J-aggregates have a

strong and narrow excitonic absorption band that is red-shifted with respect to the monomer absorption band [15]. The special way of molecular stacking, responsible for the formation of Frenkel excitons, has been extensively studied [16–24] as these aggregates are the most famous spectral sensitizers of silver halides for the photographic industry [25]. On the other hand, it has been shown that the combination of J-aggregates and silver or gold NPs provides a platform for the fundamental studies of excitons and their interaction with high electromagnetic fields, as well as a way to utilize optical properties of such a hybrid system for nanoscale optical devices.

A necessary condition for the interaction to occur is that the dye molecules are adsorbed on the surface of the NPs. Therefore, the adsorption process plays one of the key roles in these systems. The most common way in which the dye–NP hybrid systems are prepared is by mixing the appropriate colloid and dye solutions and letting the resulting mixture reach its metastable or stable state in which the NPs have dye molecules adsorbed on their surface. The dynamics of the adsorption process is quite complex as it depends on various factors including the target concentration of the constituents, affinity of the dye molecules to bind to the NP surface and the type of capping anions protecting the surface of the NPs. For instance, the spectrophotometric studies of thiocyanine (TC) dye coated silver nanoparticles (AgNPs) in Refs. [26,12–14]

\* Corresponding author.

E-mail address: [isicg@ipb.ac.rs](mailto:isicg@ipb.ac.rs) (G. Isić).

show that the capping anions can influence the mechanism of the adsorption process and therefore its efficiency.

The influence of capping anions on the adsorption process can be studied on a nanoscopic level by exploiting very strong localized plasmonic fields at the NP surface and employing surface-enhanced Raman scattering (SERS) [27,28]. SERS has already been used for identification of TC J-aggregates and for studying their dynamics on the surface NP clusters in solutions [29–36].

In view of the significance of the dye-to-NP adsorption mechanism, here the mechanism of TC dye adsorption on the surface of AgNP clusters with citrate anion stabilization is investigated. In order to probe the presence of TC dye molecules on the nanoscale (i.e. on individual AgNP clusters), Ag colloids are mixed with TC dye solutions, and subsequently drop-cast onto freshly cleaved mica or SiO<sub>2</sub> substrates and, after drying, investigated using colocalized Raman microspectroscopy and atomic force microscopy (AFM). The key mechanism used for the identification of a small amount of TC dye molecules adsorbed on AgNP clusters is SERS [32]. The measurements are complemented by rigorous numerical simulations of plane wave scattering on AgNP clusters, showing that the electromagnetic enhancement of the Raman signal originates dominantly from the nanogaps between adjacent AgNPs within the clusters. The analysis of the SERS spectra acquired at the AgNP clusters on mica substrate and the fact that the majority of the SERS signal comes from the nanogaps indicate that the citrate anions impede the efficient dye adsorption.

## 2. Materials and methods

### 2.1. Chemicals

Silver nitrate (AgNO<sub>3</sub>), potassium chloride (KCl), and sodium borohydride (NaBH<sub>4</sub>) trisodium citrate (Na<sub>3</sub>C<sub>6</sub>H<sub>5</sub>O<sub>7</sub> × 3H<sub>2</sub>O) of the highest purity were purchased from Sigma Aldrich and used as received.

Thiacyanine dye (3,3-disulfopropyl-5,5-dichlorothiacyanine sodium salt, TC) was purchased from Hayashibara Biochemical Laboratories, Okayama, Japan.

### 2.2. Samples

Aqueous solutions of borate- and citrate-capped AgNPs were synthesized by NaBH<sub>4</sub> reduction of AgNO<sub>3</sub>, as described in Refs. [12,14]. For the synthesis of citrate-capped AgNPs, Na<sub>3</sub>C<sub>6</sub>H<sub>5</sub>O<sub>7</sub> × 3H<sub>2</sub>O was used as a stabilizing agent. The solution of borate-capped AgNPs was prepared immediately before use as the colloid is stable only up to a few hours. Oppositely, the solution of citrate-capped AgNPs is stable for a longer period of time, measured in months, due to the protective citrate anion mantle. The average diameter of both borate- and citrate-capped AgNPs is around 10 nm (see Section S1 of the Supplementary information). The nominal concentration of citrate-capped AgNPs in water solution is  $c_{\text{Ag}} = 16 \text{ nM}$  (see Fig. S1 for the related absorption spectra).

Aqueous TC dye solution with nominal concentration  $c_{\text{TC}} = 50 \mu\text{M}$  of TC and 1 mM of KCl was prepared by dissolving the solid TC in water and by adding KCl afterwards. Water purified with a Millipore Milli-Q water system was used in all cases. The absorption spectra of the TC dye is given in Fig. S1 in the Supplementary information.

The Ag colloid and the TC dye solution are mixed, and the resulting mixture (see Fig. S1 in the Supplementary information for the related absorption spectra) is drop-cast on a substrate. The adsorption of TC molecules on the surface of borate-capped AgNPs happens almost instantaneously [13,12], and the mixture was therefore drop-cast on the substrate a few minutes after mix-

ing the two solutions. On the other hand, the adsorption of TC dye on the surface of citrate-capped AgNPs is a much slower process [26,14] and for that reason the mixture was left overnight and afterwards drop-cast on a substrate.

For the investigation of TC/citrate-capped AgNP clusters, as well as for initial characterization of pristine citrate-capped AgNP clusters, mica was used as a substrate. Mica has an atomically flat, hydrophilic surface on which the AgNPs are easily deposited, while its contribution to the total Raman signal is small (see Section S2 of the Supplementary information). In addition to mica, highly oriented pyrolytic graphite (HOPG) and SiO<sub>2</sub> substrates were used as their surfaces are hydrophobic and, therefore, facilitate the formation of large, closely spaced AgNP clusters as well as more efficient aggregation of the TC dye on their surface. In particular, HOPG is used for Raman characterization of concentrated TC dye, since the dye efficiently aggregates on its surface. The SiO<sub>2</sub> is used for the control study of AgNPs having dye/borate anions conformed to their surface, since the large closely spaced AgNP clusters are required for fast Raman/SERS characterization of the initially unstable borate-capped AgNPs. Raman spectra of the TC dye, Mica, Si and HOPG are shown in Fig. S2 in the Supplementary information.

### 2.3. Methods

The AgNP clusters on a substrate are investigated using colocalized Raman microspectroscopy and AFM. The two techniques are used simultaneously thus providing spatially resolved chemical information of the sample along with its surface topography at the same place. In this way one is able to identify and assert the size of the SERS active AgNP clusters while obtaining the chemical identity of the analyte adsorbed on the surface of AgNPs. The AFM is operated in tapping mode in order to minimize the lateral force between the tip and the sample induced by lateral movements of the tip across the sample. The cantilever-tip system is oscillated at the characteristic first order resonance which is usually in the 90–230 kHz range. For Raman spectroscopy and SERS measurements a linearly polarized semiconductor laser operating at a wavelength of 532 nm is used. The laser power was varied from 2 to 0.2 mW within the  $\sim 0.3 \times 0.3 \mu\text{m}$  sized focus. The experiments are performed using commercial NTegra Spectra system from NT-MDT.

To numerically solve the classical Maxwell equations we have used the finite element method implemented within the Comsol Multiphysics software package [37]. We consider clusters of AgNPs having a diameter of 10 nm on a substrate under plane wave illumination. The Ag dielectric constant is taken from Rakic et al. [38]. The substrate is assumed to be semi-infinite and isotropic with a dielectric constant of 2.25, which roughly corresponds to the dielectric constants of both mica and SiO<sub>2</sub> at visible frequencies. The surrounding medium is vacuum and its dielectric constant is 1. For purposes of efficient meshing, AgNPs are assumed to lie 1 nm above the substrate. The clusters are formed in the plane which is parallel to the substrate by allowing AgNPs to have random position but enforcing the following conditions: (i) there is a certain minimal allowed distance  $d$  between two AgNPs; two AgNPs separated by the minimal distance are said to be adjacent; (ii) each AgNP must be adjacent to at least one other AgNP, thus ensuring that each randomly generated cluster is connected. By imposing these two conditions, we were able to randomly generate various cluster geometries and mimic the lack of control over the clusters morphology in the experiment.

The absorption  $\sigma_a(\lambda)$ , scattering  $\sigma_s(\lambda)$  and extinction  $\sigma_{\text{ext}}(\lambda)$  cross sections are calculated as a function of wavelength  $\lambda$ , according to their well-known definition [39]. The electric-field enhancement  $f(\mathbf{r}, \lambda)$  is defined as the squared ratio of magnitudes of the local electric field  $\mathbf{E}_L(\mathbf{r}, \lambda)$  and the incoming electric field  $\mathbf{E}_0(\lambda)$ , with  $\mathbf{r}$  denoting the coordinate at which the former is evaluated.

Following Kerker et al. [40], the SERS enhancement factor is defined as  $F(\mathbf{r}, \lambda_{\text{inc}}, \lambda) = f(\mathbf{r}, \lambda_{\text{inc}}) / f(\mathbf{r}, \lambda)$  with  $\lambda_{\text{inc}}$  and  $\lambda$  denoting the laser and Stokes wavelength, respectively. Since the measured PL/Raman signal being reported in this paper originates from large (relative to a cluster), diffraction limited, spots of 300 nm approximate diameter, it cannot be directly related to the spatially-resolved field and SERS enhancement factors. Instead, we consider their integrals over the cluster surface  $S$  and the corresponding cluster-averaged SERS factor  $\langle F(\lambda_{\text{inc}}, \lambda) \rangle$  defined as

$$\langle F(\lambda_{\text{inc}}, \lambda) \rangle = \frac{1}{S} \int_S F(\mathbf{r}, \lambda_{\text{inc}}, \lambda) dS. \quad (1)$$

### 3. Results and discussion

#### 3.1. Surface-enhanced Raman spectroscopy of pristine citrate-capped AgNPs

Fig. 1(a) shows an AFM topograph of pristine AgNP clusters on mica surface. The corresponding PL/Raman map is shown in Fig. 1(b). The intensity of every pixel in the PL/Raman map is obtained by dividing the sum of PL/Raman intensities across the entire spectral range (100–2000  $\text{cm}^{-1}$ ) with the number of spectral points. The color bar in panel (b) thus enumerates the average photon count. Bright areas in Fig. 1(b) represent the regions of enhanced signal, henceforth referred to as hotspots. These regions coincide with AgNP clusters consisting of a large number of AgNPs (with diameters in the 10–50 nm range), as seen by comparing the PL/Raman map with the AFM topography image. In fact, we find that the hotspots are dominantly formed within larger AgNP clusters,

such as those in Fig. 1(a), regardless of the substrate which is used (mica,  $\text{SiO}_2$  or HOPG).

Fig. 1(d) and (e) shows two sets of consecutively acquired spectra with a 40 s time step taken at two hotspots from Fig. 1(b) using 532 nm laser with intensity of  $\approx 200 \mu\text{W}/\mu\text{m}^2$ . The spectra in panels (c) and (d) are similar, but cannot be quantitatively compared. Both sets feature a wide background which spreads over the entire spectral range, and a pronounced band blinking in the 1000–1800  $\text{cm}^{-1}$  range (shaded region) which hinders a quantitative analysis. Considering that citrate anions are used for stabilizing the AgNPs, our hypothesis is that the blinking spectra is the SERS signal from the citrate anion mantle, sensitive to local heating in hotspots due to the small size of citrate anions, while the wide background is PL coming from the AgNP clusters.

#### 3.2. Numerical simulations of light scattering on random AgNP clusters

In order gain an insight into hotspot formation and assess the Raman enhancement factors, we employ a numerical model to calculate the electromagnetic fields scattered on randomly generated AgNP clusters. The motivation for considering random AgNP clusters is to get an idea on the variability of the electric field enhancement upon changing the cluster geometry and to identify any invariants which could be used to interpret SERS measurements on clusters whose exact geometry is unknown. A typical cluster consisting of 20 AgNPs is shown in Fig. 2(a). In this example we set the minimal AgNP distance at  $d = 0.8 \text{ nm}$  while the adjacent AgNPs are indicated by solid (red) lines Fig. 2(a). The extinction cross-section of the AgNP cluster in panel (a) is plotted in Fig. 2(b),

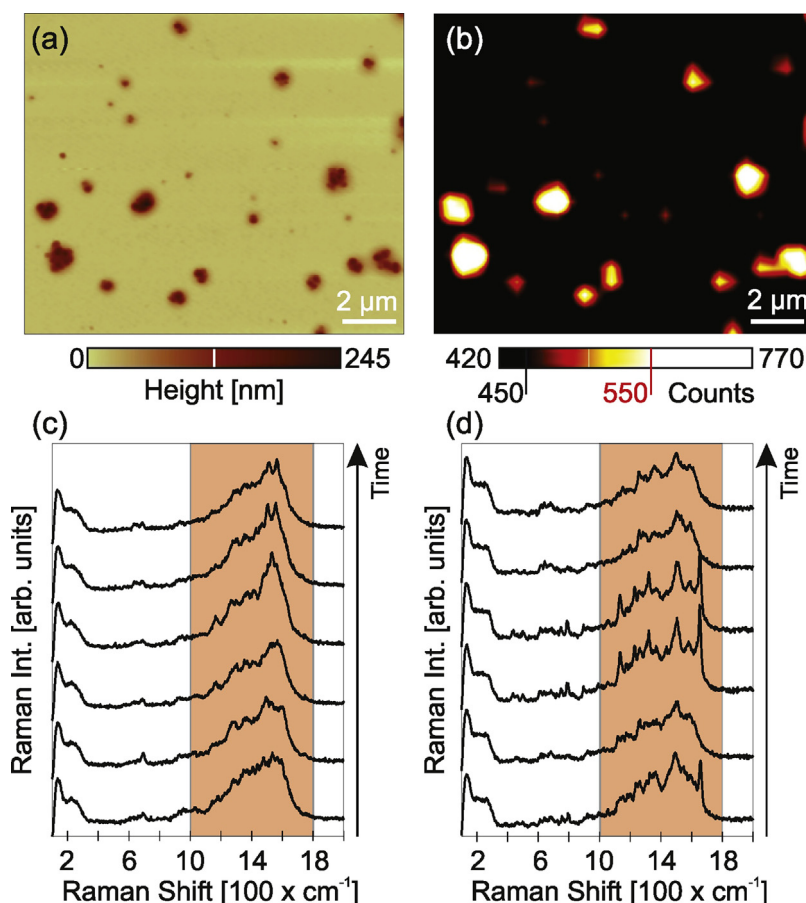


**Fig. 1.** (a) AFM topograph of pristine AgNP clusters drop-cast onto a freshly-cleaved mica substrate. (b) Corresponding PL/Raman map. (c), (d) Typical SERS spectra acquired within two hot spots in panel (b). The spectra were measured consecutively with a 40 s time step. The excitation laser wavelength is 532 nm.

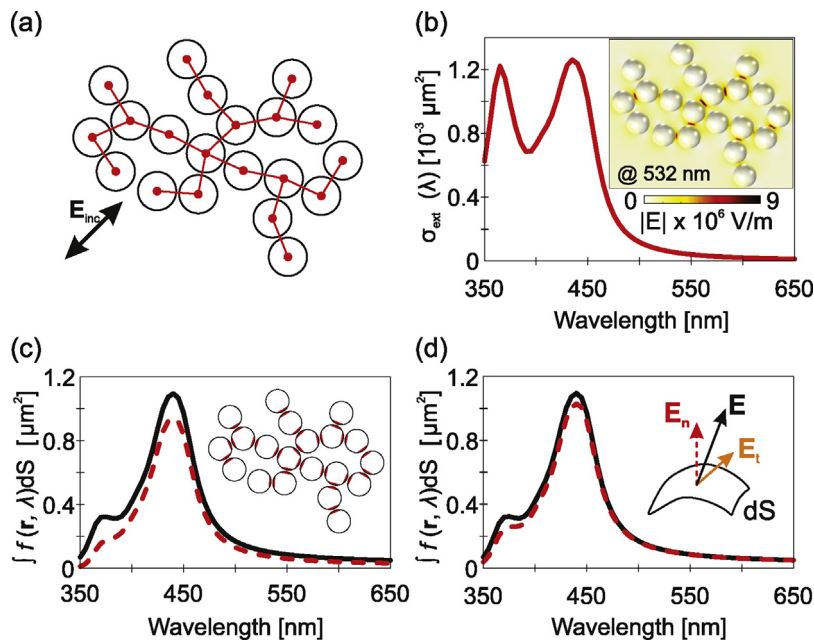


**Fig. 2.** (a) Sketch of a typical cluster geometry used in the numerical model. Normal incidence is assumed for the incoming wave while its electric field is polarized parallel to the plane of the cluster and oriented as indicated by the arrow. The incident field intensity is set to  $200 \mu\text{W}/\mu\text{m}^2$ . (b) Extinction spectra of the cluster in panel (a). The inset shows the electric field magnitude distribution at 532 nm. (c) Surface integrals of the intensity enhancement over the entire cluster surface (solid black line) and over the entire gap area (dashed red line) plotted as the function of the wavelength. (d) Surface integrals of the total field enhancement (solid, black) and the ratio of the field component perpendicular to the AgNP surface (dashed, red) both taken over the entire cluster surface. (For interpretation of the references to color in this legend, the reader is referred to the web version of the article.)

as a function of the incident wavelength. For the considered cluster, the scattering cross-section is negligible with respect to the absorption cross-section and therefore  $\sigma_{\text{ext}} \approx \sigma_{\text{a}}$ . The two peaks observed at 365 and 435 nm, represent the single particle and cluster surface plasmon, respectively. Below we find that the wavelength of the former is virtually independent on the presence of other AgNPs, while the cluster plasmon wavelength redshifts with increasing cluster size. Upon the excitation of a cluster plasmon, the electric field is resonantly enhanced over the entire cluster. Although the distribution of resonant fields is highly dependent on the details of AgNP arrangement [41], the highest enhancement is known [42,43] to be invariably reached within the gaps between adjacent AgNPs, which is corroborated by our numerical simulations of many random AgNP arrangements.

The inset of Fig. 2(b) shows the spatial distribution of the electric field magnitude in the plane containing the NP centers, excited at 532 nm which is far from the cluster plasmon at 435 nm. This hints that the highest field enhancements are reached in NP gaps for any wavelength and not just for resonances. Fig. 2(c) shows the surface integral of the field enhancement evaluated over: (i) the entire cluster surface, consisting of the surfaces of all AgNPs and (ii) over the entire gap area, consisting of the sum of gap areas of individual AgNPs, defined as parts of the NP surface located very close to the adjacent AgNP, as indicated by the (red) shading in Fig. 2(c) inset. According to this definition, the surface over which the (ii) integral is evaluated is a small fraction of the (i) integral. However, the spectra in Fig. 2(c) show that these integrals have virtually the same value away from surface plasmon resonances. The difference around the cluster plasmon wavelength is also not significant, being of the order of 10%. This shows that regardless of the cluster geometry, the majority of the SERS signal of any species adsorbed uniformly on AgNPs is likely to come from the gap region (see also Fig. S3 in the Supplementary information).

Another important question regarding the fields on AgNP clusters is their orientation with respect to the AgNP surface, as

it determines the SERS cross section of vibrational modes of molecules adsorbed on the AgNP surface. To evaluate the extent to which the electric field is perpendicular to the local surface, in Fig. 2(d) we evaluate the surface integrals (taken over the entire cluster) of (i) the square of the normalized total electric field magnitude, which equals  $f(\mathbf{r}, \lambda)$  by definition (solid, black), and (ii) the square of the normalized magnitude of the electric field component perpendicular to the AgNP surface (dashed, red). The comparison of the two spectra in Fig. 2(d) shows that the contribution of the tangential component of the local electric field is negligible, indicating that in such clusters the perpendicular component of the electric field is the principal source of the SERS signal.

Having established that for an arbitrarily chosen AgNP cluster the large majority of the SERS signal comes from gaps between AgNPs and is associated with the perpendicular electric field component, we now focus on the cluster-averaged SERS enhancement factor  $\langle F(\lambda_{\text{inc}}, \lambda) \rangle$  and investigate how is it affected by the cluster size and geometry. The typical case is illustrated in Fig. 3(a) in which we consider a hierarchy of 3 NP clusters shown in the inset, each having twice as many AgNPs as the previous one. The first one represents a randomly chosen connected arrangement of 5 AgNPs with  $d = 0.8$  nm. The second is obtained by adding 5 more AgNPs so that each new AgNP is adjacent to one of the existing AgNPs. Finally, the third and largest cluster is obtained by adding 10 more AgNPs to the second one. The corresponding  $\langle F(\lambda_{\text{inc}}, \lambda) \rangle$  spectra in Fig. 3(a) shows two main effects of the cluster size increase. First, the enhancement peaks associated with the cluster plasmon undergoes a gradual redshift. Second, the surface-average enhancement  $\langle F(\lambda_{\text{inc}}, \lambda) \rangle$  increases, meaning that the actual SERS signal enhancement given by  $S \times \langle F(\lambda_{\text{inc}}, \lambda) \rangle$  will increase even more rapidly with adding new particles to the cluster. For example, a cluster having 5 AgNPs exhibits an average Raman enhancements of the order of 10 in the 532–600 nm range, whereas a cluster having 20 AgNPs yields 10 times higher values in the same range. In previous studies on AuNP chains [44], the increase of particle number has been found



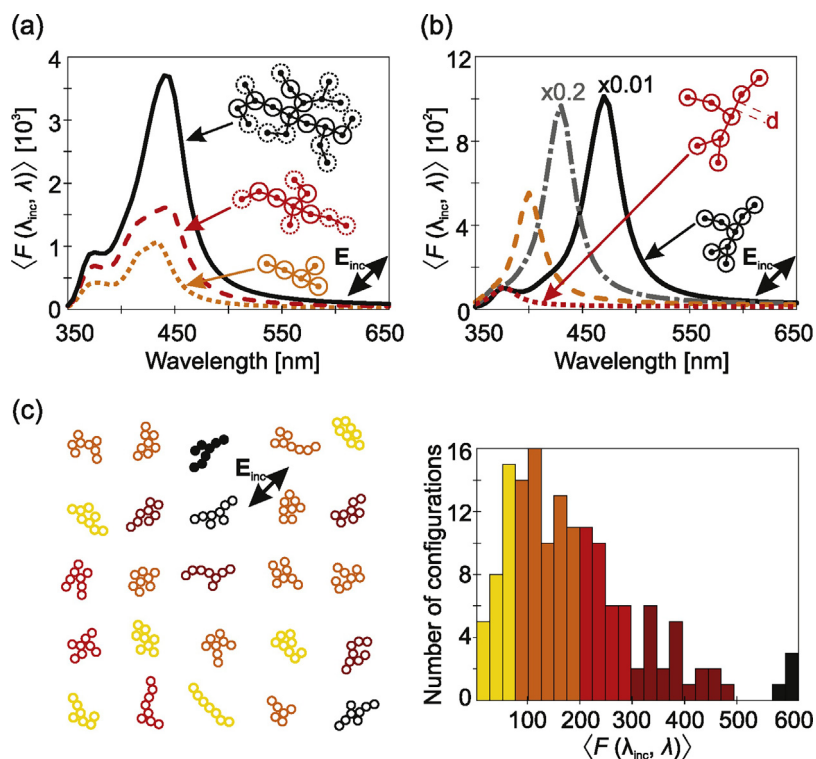


**Fig. 3.** (a) The average Raman enhancement calculated as a function of the emission wavelength for clusters having 5 particles (dotted orange line), 10 particles (dashed red line) and 20 particles (solid black line). (b) The average Raman enhancement calculated as a function of the emission wavelength for a cluster with 8 particles when the minimal distance between the particles is varied. Particles connected by lines, in the inset, are at the minimal distance  $d$  from each other. Solid (black) line corresponds to  $d = 0.5$  nm, whereas dash-dotted (gray) line, dashed (orange) line and dotted (red) line correspond to  $d = 1$  nm,  $d = 2$  nm and  $d = 5$  nm, respectively. (c) The left panel shows some of the 150 considered cluster variants and the electric field polarization direction. All the clusters have 8 particles, with the minimal distance  $d = 0.8$  nm. The right panel shows a histogram of the average Raman enhancement calculated at the emission wavelength 550 nm for all 150 cluster variants. In all calculations normal incidence at a wavelength 532 nm and the incident field intensity of  $200 \mu\text{W}/\mu\text{m}^2$  are assumed. (For interpretation of the references to color in this legend, the reader is referred to the web version of the article.)

to either increase or decrease the average Raman enhancement, depending on the relative position of the incident wavelength and the cluster (chain) plasmon.

In Fig. 3(b) we consider the role of the spacing  $d$  between adjacent AgNPs. For a cluster comprising 8 AgNPs decreasing  $d$  from 5 nm down to 0.5 nm is seen to result in drastic changes of  $\langle F(\lambda_{\text{inc}}, \lambda) \rangle$ . The cluster plasmon is rapidly blueshifted and approaches the single-particle plasmon as the AgNPs are moved further apart (see also panel (c) of Fig. S3 in the Supplementary information). Similar conclusions have been previously reported for the AuNP linear chains embedded in a dielectric medium [42,45]. Meanwhile, the peak values of  $\langle F(\lambda_{\text{inc}}, \lambda) \rangle$  are seen to decrease very rapidly since the gap field enhancement becomes less effective with increasing  $d$ . For example, the lowest considered minimal distance of 0.5 nm yields SERS enhancements as high as  $10^4$  in the 532–600 nm range.

Lastly, by evaluating the average Raman enhancement at the excitation and Stokes wavelengths of 532 nm and 550 nm, respectively, for a 150 randomly generated 8 AgNP clusters, we evaluate how the cluster morphology affects the non-resonant SERS enhancement value. The variety of clusters that have been considered in the 150 member ensemble, is represented by 25 typical members sketched in the left panel of Fig. 3(c). The histogram of  $\langle F(\lambda_{\text{inc}}, \lambda) \rangle$  values is shown in the right panel, where the column colors are selected so that they correspond to the color of the associated cluster in the left panel. The distribution is quite wide, spanning the range from 50 to 600. By comparing the two panels of Fig. 3(c), we see that the highest enhancements are reached in chain shaped clusters having the chain axis aligned with the incident electric field, such as the one illustrated in Fig. 3(c) by filled circles. The effect of disorder of the linear AuNP chain on the Raman

enhancement was studied in Ref. [43], where increasing disorder was found to diminish the Raman enhancement. In this case, the highest Raman enhancements were found for AuNP chains, when the incident electric field is oriented along the chain axis.

The brief numerical analysis of light scattering on random AgNP clusters made in this section shows that the overall SERS enhancement is highly dependent the cluster geometry and its orientation relative to the electric field polarization. The sensitivity of  $\langle F(\lambda_{\text{inc}}, \lambda) \rangle$  to fine details, such as the gap spacing, makes its exact evaluation very difficult even when electron microscopy is used for determining the AgNP arrangement with nanometer spatial resolution [46]. In the present case, the possibility of resonant enhancement cannot be excluded, since the cluster plasmon resonances are seen to redshift in elongated clusters with a larger number of particles than the ones considered here [42,43]. However, beside the well elaborated enormous Raman enhancements having a resonant origin [42], we have shown that in the non-resonant case enhancement factors in the range of  $10^2$ – $10^3$  are to be expected.

### 3.3. Surface-enhanced Raman spectroscopy of TC coated AgNPs I: influence of citrate capping anions on the TC dye adsorption

In the TC/AgNP mixture, the AgNPs may have the J-aggregates or dye monomers or dimers adsorbed on their surface, or even remain pristine. Therefore, it is expected that AgNP clusters drop-cast from the mixture would have a variety of SERS spectra corresponding to those of different dye conformations, citrate anions and even their combinations. To make a clear distinction between the non-aggregated and aggregated molecules one must have an

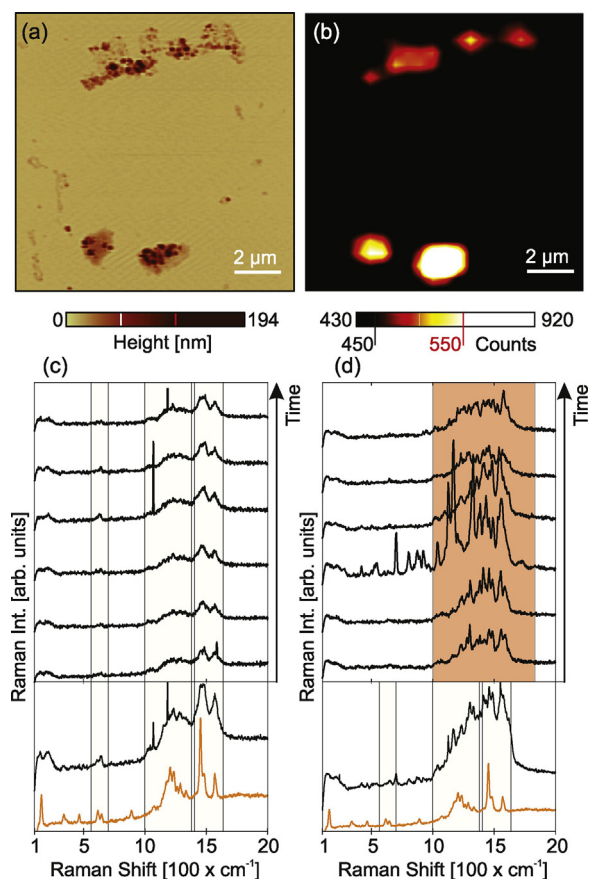


**Fig. 4.** (a) AFM topograph of TC dye coated Ag NP clusters which are drop-cast on mica. (b) Corresponding PL/Raman map. (c) and (d) Typical SERS spectra acquired within the hot spots, by consecutive measurements with 40 s time step. The excitation laser wavelength is 532 nm. In the lower parts of panels (c) and (d) shown are the SERS spectra obtained by summation of the corresponding consecutively acquired spectra, and the Raman spectra of the drop-cast TC dye. (For interpretation of the references to color in this legend, the reader is referred to the web version of the article.)

excitation resonant with the absorption of either aggregated or non-aggregated dye molecules [32,47]. Here we use a non-resonant laser line at 532 nm which does not allow identification of different dye conformations. However, AgNP clusters are very efficient enhancers at this wavelength, as it is shown in Section 3.1 and thus through the SERS effect alone we are able to determine if the TC dye molecules are adsorbed on AgNPs or not.

Comparison of the AFM topograph and the corresponding Raman map in Fig. 4(a) and (b) reveals that the hot spots are located within the larger AgNP clusters, as in the case of pristine AgNPs in Section 3.1. The SERS spectra acquired at these hot spots can be unambiguously categorized in two groups: one featuring stable Raman bands during successive measurements and the other having blinking Raman bands. The wide background from the AgNP clusters exists in this case as well. Fig. 4(c) and (d) shows the two distinct spectra types. The recording time step is 40 s and the laser intensity is  $\approx 200 \mu\text{W}/\mu\text{m}^2$ .

The consecutively measured SERS spectra having stable Raman bands are reminiscent of the drop-cast TC dye Raman spectrum. The similarity between the two becomes even more convincing after summation of ten consecutively measured spectra, six of which are displayed in Fig. 4(c). By applying markers to the three wave-number regions, I (300–1000  $\text{cm}^{-1}$ ), II (1050–1250  $\text{cm}^{-1}$ ), III (1400–1600  $\text{cm}^{-1}$ ), where the TC dye has its characteristic Raman bands (see Fig. S2 in the Supplementary information), we find that in region I around 600  $\text{cm}^{-1}$  the summed SERS spectrum has

two bands matching those of a drop-cast TC dye, which is plotted again, for clarity, below the summed spectrum. The modes around 400  $\text{cm}^{-1}$  and 900  $\text{cm}^{-1}$  are, however, absent in the related TC dye SERS. In the remaining regions II and III the two spectra have, more or less, the same Raman bands and even similar backgrounds. Hence, our experiments corroborate the fact that the dye molecules are adsorbed on the surface of the AgNPs, and point out another interesting possibility – the dye molecules drop-cast on the surface of HOPG may be similarly organized as the dye molecules on the surface of the AgNPs.

Panel (d) in Fig. 4 displays SERS spectra characterized by a pronounced band blinking in the 1000–1800  $\text{cm}^{-1}$  range, as indicated by gray (orange) region. The resemblance of the spectra in Fig. 4(d) and those of pristine AgNPs in Fig. 1(c) and (d) suggests that the TC dye molecules are not adsorbed on the surface of the AgNPs. However, the sum of the consecutive recordings, shown in the lower part of Fig. 4(d), reveals certain SERS bands in region II and III which are overlapping the drop-cast TC dye bands. Occasional emergence of Raman bands which could belong to the TC dye bands in regions I, II and III, however, is a common event even for the SERS spectra of pristine AgNPs. Having in mind that practically the entire enhanced Raman signal originates from the analyte located in the nanogaps, the blinking SERS signal can be interpreted as a consequence of mixing of the pristine AgNPs blinking SERS and the TC dye SERS which are collected at different nanogaps where the former has the dominant contribution. Consequently, we are unable to conclude whether the AgNP clusters exhibiting blinking SERS bands have the dye molecules adsorbed on their surface or not. However, the existence of the two distinct SERS spectra clearly points out that the AgNPs are partially covered by the TC dye molecules. This further indicates that during the adsorption process, the TC dye molecules are either competing with citrate anions in order to replace them on the surface of AgNPs or that the TC dye molecules have a difficulty conforming over the citrate anion mantle. Hence, we proceed further by changing the concentration of TC dye in the mixture while maintaining the concentration of AgNPs constant at  $c_{\text{Ag}} = 16 \text{ nM}$ .

The blinking and TC dye SERS spectra observed for  $0.01c_{\text{TC}} = 0.5 \mu\text{M}$ ,  $0.1c_{\text{TC}} = 5 \mu\text{M}$ , and  $0.5c_{\text{TC}} = 25 \mu\text{M}$  of TC, are shown in Fig. 5(a)–(c), respectively. By analyzing spectra at the hotspots within various Raman maps, we find that the AgNP clusters deposited from the solution with the lowest dye concentration yield no clear dye SERS spectra, whereas the AgNP clusters deposited from the solution with the two higher dye concentration provide a number of distinct TC dye SERS spectra at the hotspots, shown in Fig. 5. Comparison of the summed SERS spectra, in the lower parts of panels (a), (b) and (c) in Fig. 5, and the concentrated TC dye Raman spectra corroborates that the SERS spectra in panels (b) and (c) correspond to the one of the TC dye. As expected, using TC dye concentrations of  $0.01c_{\text{TC}} = 0.5 \mu\text{M}$ ,  $0.1c_{\text{TC}} = 5 \mu\text{M}$  in the final solution yields either pristine or partially covered AgNP clusters, a fact that concurs with the results in Ref. [14]. However, observation of the blinking type SERS within the AgNP clusters derived from the mixture with the highest TC dye concentration of  $0.5c_{\text{TC}} = 25 \mu\text{M}$ , for which all of the AgNPs in the solution should be covered by the dye molecules [14], further indicates that the citrate anion mantle impedes the adsorption of the TC dye molecules.

### 3.4. Surface-enhanced Raman spectroscopy of TC coated AgNPs II: influence of borate and citrate capping anions on the TC dye adsorption

In order to examine if the citrate anions impede the TC dye adsorption, we have performed an additional set of measurements on a control sample – borate-capped AgNPs mixed with the TC dye and deposited on the surface of 300 nm thick  $\text{SiO}_2$ , which is thermally grown on the Si wafer. Meanwhile, the borate-capped AgNPs

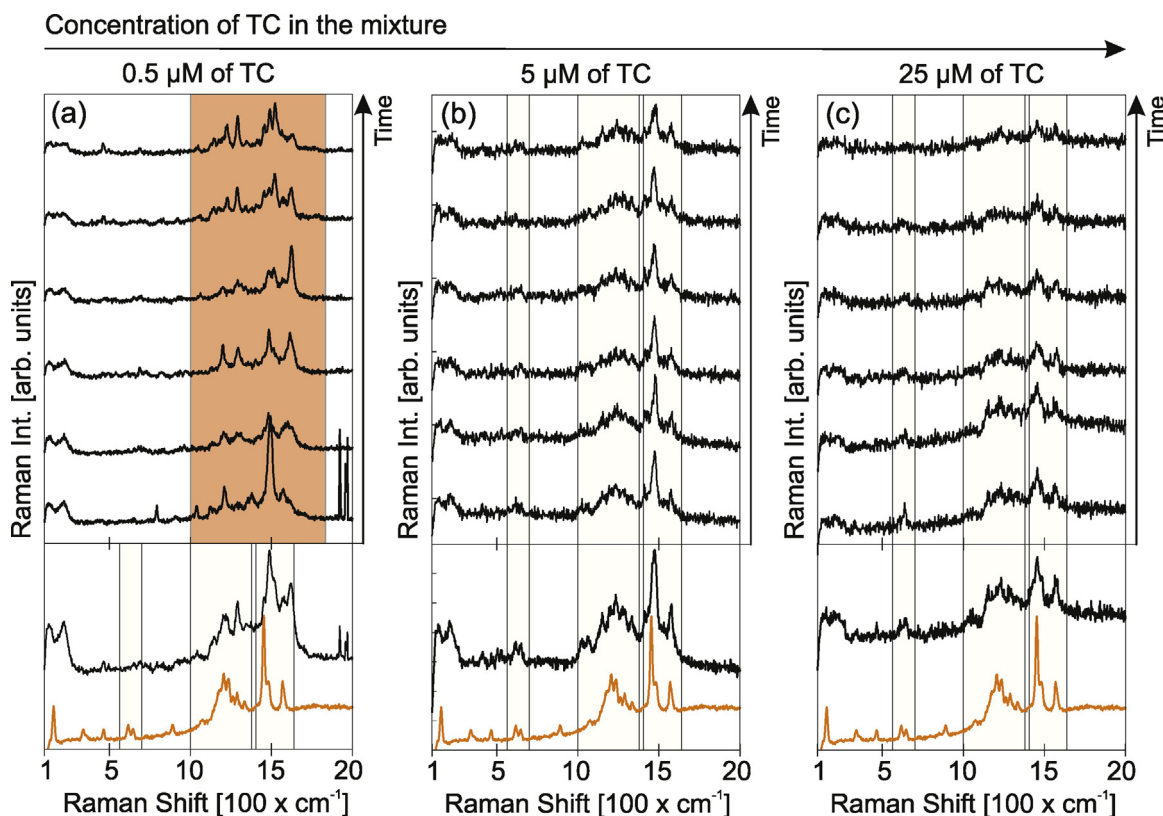


**Fig. 5.** Blinking and TC dye SERS spectra (acquired by consecutive measurements with 40 s time step) at hotspots on the samples made by varying the TC concentration in TC-Ag NP mixture: (a) 0.5  $\mu\text{M}$ , (b) 5  $\mu\text{M}$  and (c) 25  $\mu\text{M}$ . All shown spectra were taken under the same conditions using 532 nm laser with intensity of  $200 \mu\text{W}/\mu\text{m}^2$ .

are unstable with the average lifetimes of the order of couple of hours in the colloid dispersion and are usually stabilized by sodium citrate (or rather by the citrate anions which replace the borate anions while conforming to the surface of the AgNPs), as explained in Ref. [14]. The related lifetimes are much shorter upon deposition of these AgNPs on a substrate. The  $\text{SiO}_2$  surface is hydrophobic, and, therefore, promotes formation of closely spaced clusters larger than those observed on mica, since the droplet drop-cast of the former dries over a certain area rather than spreading all over the surface. Such an arrangement, along with the enhanced contrast between the  $\text{SiO}_2$  surface and the clusters, is absolutely necessary for fast acquisition of the SERS signal from the unstable, dye/borate-capped AgNP clusters.

Fig. 6(a)–(c) shows the three Raman maps corresponding to: (i) AgNP clusters deposited on mica from a solution having a (citrate-capped) AgNP to the TC dye concentration ratio of  $22 \text{ nM}/17 \mu\text{M} \approx 1.3 \times 10^{-3}$ , (ii) AgNP clusters deposited on mica from a solution having a (citrate capped) AgNP to the TC dye concentration ratio of  $16 \text{ nM}/25 \mu\text{M} \approx 0.64 \times 10^{-3}$ , (iii) AgNP clusters deposited on  $\text{SiO}_2/\text{Si}$  from a solution having a (borate-capped) AgNP to the TC dye concentration ratio of  $10 \text{ nM}/16 \mu\text{M} \approx 0.63 \times 10^{-3}$ , respectively. The (red) diamonds mark the spatial positions within the hotspots where the blinking type of Raman spectra is observed, whereas the (green) squares mark the pixels having the TC dye type of Raman spectra. These maps share the color bar which is located below them. Panels (d), (e) and (f) of Fig. 6 display examples of the spectra collected at the hotspots within the corresponding maps in panels (a), (b) and (c), respectively. For comparison, the concentrated TC dye Raman spectra is plotted in each panel, below all the other spectra.

The dye/borate-capped AgNPs deposited on the  $\text{SiO}_2/\text{Si}$ , form a higher number of larger clusters than the dye/citrate-capped AgNPs on mica, as seen by comparing the Raman maps in panels (a), (b)

and (c), as expected. The SERS spectra acquired at these clusters is exclusively of the TC dye type, as seen in panel (c). In fact, we find this to be the case for every recorded Raman map. In contrast, the dye/citrate-capped AgNP clusters exhibit both the blinking and the TC dye SERS, even when the ratio of the citrate-capped AgNPs and the TC dye concentrations in solution is approximately the same as the one of the borate-capped AgNPs and the TC dye (compare panels (b) and (c) in Fig. 6). The adsorption of the TC dye seems to be more efficient if the AgNPs have borate anions initially conformed to their surface and, therefore, we conjecture that the citrate anions indeed interfere with the adsorption process of the TC dye molecules.

Our findings are in agreement with the previous spectrophotometric study of J-aggregation of TC dye on the surface of AgNPs [26,13,14,12], where is found that the capping anions (borate or citrate), as well as added KCl, have an important role in the adsorption and J-aggregation of the dye molecules. In case of borate-capped AgNPs, the J-aggregation is found to be a fast process ( $k_{\text{app}} = 4.97 \text{ s}^{-1}$ ) whose kinetics can be explained in terms of autocatalysis. Differently, kinetics measurements of J-aggregation on the surface of citrate-capped AgNPs has shown that the J-aggregation occurs via a two-step slower process (adsorption and aggregation,  $k_{\text{app1}} = 0.008 \text{ s}^{-1}$  and  $k_{\text{app2}} = 0.11 \text{ s}^{-1}$ ). Also, in the case of citrate-capped AgNPs was found that the quantity of added KCl has an important role in the adsorption of TC dye molecules.

This conclusion is further supported by the analysis of the DFT calculated adsorption energies of the TC dye, borate and citrate anions on the surface of Ag, reported in our previous work [26] (see also Section S4 of the Supplementary information).

#### 4. Summary

In summary, the analysis of SERS enhancement based on rigorous simulations of Maxwell equations for the case of plane wave



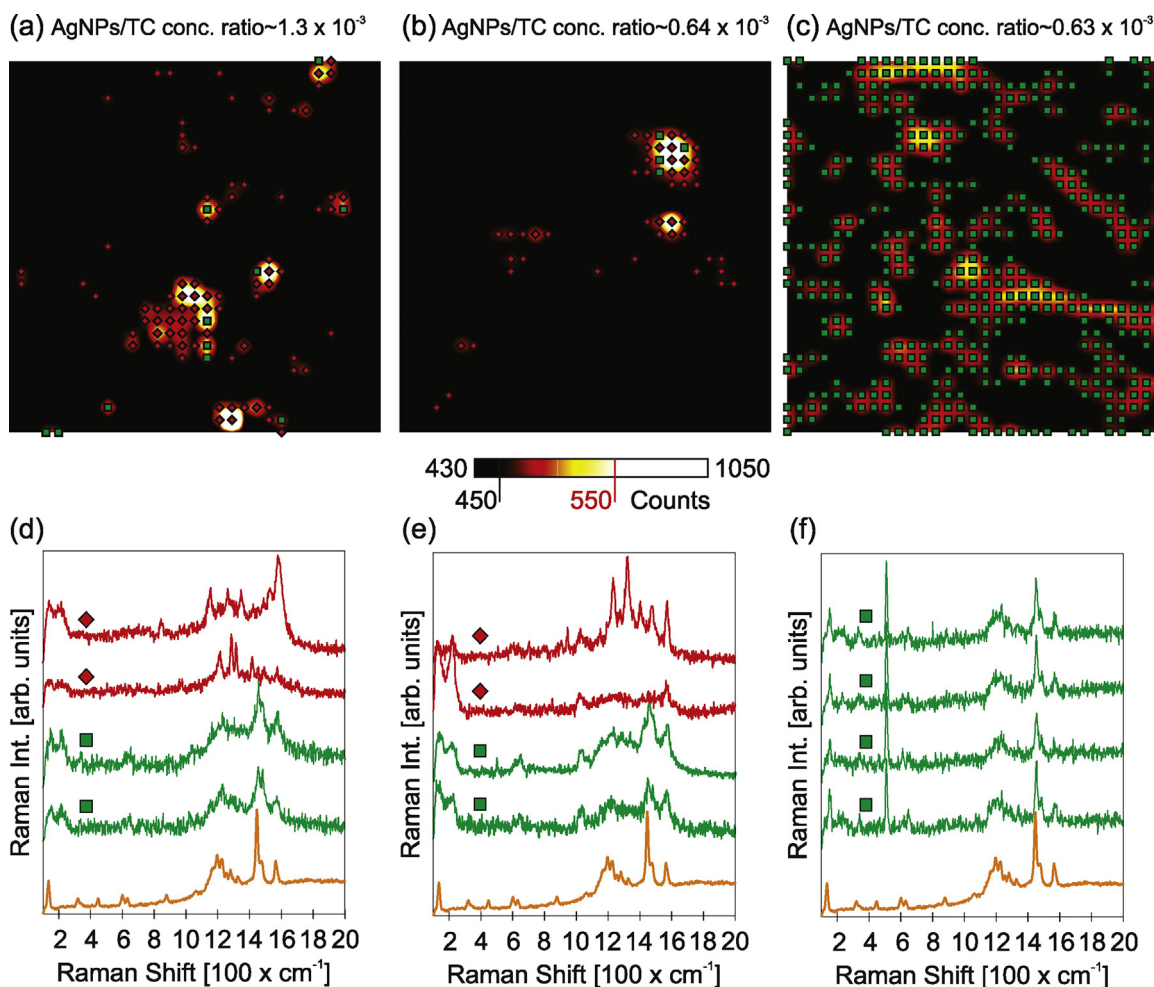


**Fig. 6.** Raman maps of (a) clusters deposited on mica from a solution having a (citrate capped) NP to the TC dye concentration ratio of 22 nM/17  $\mu$ M  $\approx 1.3 \times 10^{-3}$ , (b) clusters deposited on mica from a solution having a (citrate capped) NP to the TC dye concentration ratio of 16 nM/25  $\mu$ M  $\approx 0.64 \times 10^{-3}$  (c) clusters deposited on SiO<sub>2</sub>/Si from a solution having a (borate capped) NP to the TC dye concentration ratio of 10 nM/16  $\mu$ M  $\approx 0.64 \times 10^{-3}$ . (d)–(f) Examples of the blinking and dye SERS spectra observed in the Raman maps, displayed below the corresponding Raman maps.

scattering on random silver nanoparticle clusters on various substrates has shown that, for the investigated nanoparticles and the 532 nm excitation laser, typical enhancement factors in the range of  $10^2$ – $10^3$  can be expected. The highest field enhancement factors are reached at collective nanoparticle plasmon resonances, which lie in the 400–500 nm range for medium sized clusters (around 20 nanoparticles), and become redshifted in elongated clusters with an increasing number of particles. From an inspection of electromagnetic field distribution on nanoparticle surfaces, a conclusion is reached that at least 90% of the SERS total enhancement originates from nanogaps between adjacent nanoparticles, implying that the experiments are sensitive only to adsorbates located in these gaps.

Combined AFM and PL mapping of citrate-capped AgNP clusters with dye molecules adsorbed from solutions of variable TC concentration have shown that, even at highest TC concentrations, not all hotspots exhibit Raman signatures characteristic of TC dye molecules, indicating that the clusters are only partially covered by dye molecules. In contrast, the control experiment carried out with borate-capped AgNP clusters, with similar nanoparticle and dye concentrations, has shown a complete dye-coverage of AgNP clusters.

These results are a direct demonstration that the citrate anions, while useful for stabilizing the colloid, impede the efficient TC dye adsorption.

## Acknowledgements

The research reported in this article was supported by the Serbian Ministry of Education, Science and Technological Development through project Nos. ON171005, ON172023, III45016. This work was performed in the context of COST Action MP 1302 “Nanospectroscopy”.

## Appendix A. Supplementary data

Supplementary data associated with this article can be found, in the online version, at <https://doi.org/10.1016/j.apsusc.2017.10.148>.

## References

- [1] A. Manjavacas, F.J.G.d. Abajo, P. Nordlander, Quantum plexcitonics: strongly interacting plasmons and excitons, *Nano Lett.* 11 (6) (2011) 2318–2323.
- [2] N.T. Fofang, T.-H. Park, O. Neumann, N.A. Mirin, P. Nordlander, N.J. Halas, Plexcitonic nanoparticles: plasmon exciton coupling in nanoshell-j-aggregate complexes, *Nano Lett.* 8 (10) (2008) 3481–3487.
- [3] E. Dulkeith, A.C. Morteau, T. Niedereichholz, T.A. Klar, J. Feldmann, S.A. Levi, F.C.J.M. van Veggel, D.N. Reinholdt, M. Möller, D.I. Gittins, Fluorescence quenching of dye molecules near gold nanoparticles: radiative and nonradiative effects, *Phys. Rev. Lett.* 89 (2002) 203002–203006.
- [4] J. Zhao, X. Zhang, Y.C. Ranjit, A.J. Haes, R.P. Van Duyne, Localized surface plasmon resonance biosensors, *Nanomedicine* 1 (2006) 219–228.



- [5] M.A. Noginov, G. Zhu, A.M. Belgrave, R. Bakker, V.M. Shalae, E.E. Narimanov, S. Stout, E. Herz, T. Suteewong, U. Wiesner, Demonstration of a spaser-based nanolaser, *Nature* 460 (2009) 1110–1112.
- [6] N. Kometani, M. Tsubonishi, T. Fujita, K. Asami, Y. Yonezawa, Preparation and optical absorption spectra of dye-coated Au, Ag, and Au/Ag colloidal nanoparticles in aqueous solutions and in alternate assemblies, *Langmuir* 17 (3) (2001) 578–580.
- [7] A. Yoshida, N. Kometani, Effect of the interaction between molecular exciton and localized surface plasmon on the spectroscopic properties of silver nanoparticles coated with cyanine dye J-aggregates, *J. Phys. Chem. C* 114 (7) (2010) 2867–2872.
- [8] V.S. Lebedev, A.S. Medvedev, D.N. Vasil'ev, D.A. Chubich, A.G. Vitukhnovsky, Optical properties of noble-metal nanoparticles coated with a dye J-aggregate monolayer, *Quantum Electron.* 40 (3) (2010) 246.
- [9] Y. Kitahama, M. Kashiara, T. Itoh, Y. Ozaki, Surface-enhanced phosphorescence measurement by an optically trapped colloidal Ag nanoaggregate on anionic thiocarbocyanine H-aggregate, *J. Phys. Chem. C* 117 (6) (2013) 2460–2466.
- [10] A. Vujačić, V. Vasić, M. Dramićanin, S.P. Sovilj, N. Bibić, J. Hranisavljević, G.P. Wiederrecht, Kinetics of J-aggregate formation on the surface of Au nanoparticle colloids, *J. Phys. Chem. C* 116 (7) (2012) 4655–4661.
- [11] A. Vujačić, V. Vasić, M. Dramićanin, S.P. Sovilj, N. Bibić, S. Milonjić, V. Vodnik, Fluorescence quenching of 5,5-disulfofopropyl-3,3-dichlorothiacyanine dye adsorbed on gold nanoparticles, *J. Phys. Chem. C* 117 (13) (2013) 6567–6577.
- [12] B.B. Laban, V. Vodnik, A. Vujačić, S.P. Sovilj, A.B. Jokić, V. Vasić, Spectroscopic and fluorescence properties of silver-dye composite nanoparticles, *Russ. J. Phys. Chem. A* 87 (13) (2013) 2219–2224.
- [13] B. Laban, V. Vodnik, M. Dramićanin, M. Novaković, N. Bibić, S.P. Sovilj, V.M. Vasić, Mechanism and kinetics of J-aggregation of thiacyanine dye in the presence of silver nanoparticles, *J. Phys. Chem. C* 118 (40) (2014) 23393–23401.
- [14] B. Laban, V. Vodnik, V. Vasić, Spectrophotometric observations of thiacyanine dye J-aggregation on citrate capped silver nanoparticles, *Nanospectroscopy* 1 (2015) 54–60.
- [15] F. Würthner, T.E. Kaiser, C.R. Saha-Möller, J-aggregates: from serendipitous discovery to supramolecular engineering of functional dye materials, *Angew. Chem. Int. Ed.* 50 (15) (2011) 3376–3410.
- [16] M. Kawasaki, T. Sato, T. Yoshimoto, Controlled layering of two-dimensional J-aggregate of anionic cyanine dye on self-assembled cysteamine monolayer on Au(111), *Langmuir* 16 (12) (2000) 5409–5417.
- [17] R.W. Owens, D.A. Smith, Stm imaging of cyanine dye J-aggregates formed on carboxyl-terminated self-assembled monolayers, *Langmuir* 16 (2) (2000) 562–567.
- [18] H. Yao, S. Kitamura, K. Kimura, Morphology transformation of mesoscopic supramolecular J aggregates in solution, *Phys. Chem. Chem. Phys.* 3 (2001) 4560–4565.
- [19] N. Vranken, P. Foubert, F. Khn, R. Gronheid, I. Scheblykin, M. Van der Auweraer, F.C. De Schryver, Influence of the deposition method on the topography and spectroscopy of J-aggregates of a thiocarbocyanine dye adsorbed to a Langmuir film, *Langmuir* 18 (22) (2002) 8407–8417.
- [20] H. Yao, Y. Kagoshima, S. Kitamura, T. Isohashi, Y. Ozawa, K. Kimura, Superstructures of mesoscopic monomolecular sheets of thiacyanine J aggregates in solution, *Langmuir* 19 (21) (2003) 8882–8887.
- [21] H. Yao, T. Isohashi, K. Kimura, Large birefringence of single J-aggregate nanosheets of thiacyanine dye in solution, *Chem. Phys. Lett.* 396 (4–6) (2004) 316–322.
- [22] S. Özcelik, M.M. Demir, B. Birkan, Probing nanoscale domains of J-aggregates deposited on a mica surface, *J. Phys. Chem. B* 108 (15) (2004) 4679–4683.
- [23] H. Yao, K. Domoto, T. Isohashi, K. Kimura, In situ detection of birefringent mesoscopic H and J aggregates of thiocarbocyanine dye in solution, *Langmuir* 21 (3) (2005) 1067–1073.
- [24] V.V. Prokhorov, O.M. Perelygina, S.I. Pozin, E.I. Mal'tsev, A.V. Vannikov, A.Y. Tsivadze, Tubular structure of J-aggregates of cyanine dye, *Dokl. Chem.* 460 (1) (2015) 1–4.
- [25] T.H. James, *The Theory of the Photographic Process*, 4th ed., Macmillan, New York, 1977.
- [26] B. Laban, I. Zeković, D. Vasić Aničijević, M. Marković, V. Vodnik, M. Luce, A. Cricenti, M. Dramićanin, V. Vasić, Mechanism of 3,3-disulfofopropyl-5,5-dichlorothiacyanine anion interaction with citrate-capped silver nanoparticles: adsorption and J-aggregation, *J. Phys. Chem. C* 120 (32) (2016) 18066–18074.
- [27] M. Kerker, O. Siiman, L.A. Bumm, D.-S. Wang, Surface enhanced Raman scattering (SERS) of citrate ion adsorbed on colloidal silver, *Appl. Opt.* 19 (19) (1980) 3253–3255.
- [28] O. Siiman, L.A. Bumm, R. Callaghan, C.G. Blatchford, M. Kerker, Surface-enhanced Raman scattering by citrate on colloidal silver, *J. Phys. Chem.* 87 (6) (1983) 1014–1023.
- [29] D.L. Akins, S. Zelik, H.-R. Zhu, C. Guo, Aggregation-enhanced Raman scattering of a cyanine dye in homogeneous solution, *J. Phys. Chem. A* 101 (18) (1997) 3251–3259.
- [30] Y. Kitahama, Y. Tanaka, T. Itoh, Y. Ozaki, Wavelength-dependent surface-enhanced resonance Raman scattering by excitation of a transverse localized surface plasmon, *J. Phys. Chem. C* 113 (27) (2009) 11877–11883.
- [31] Y. Kitahama, Y. Tanaka, T. Itoh, Y. Ozaki, Time-resolved surface-enhanced resonance Raman scattering spectra of thiacyanine molecules in water, *Chem. Lett.* 38 (1) (2009) 54–55.
- [32] Y. Kitahama, Y. Tanaka, T. Itoh, M. Ishikawa, Y. Ozaki, Identification of thiacyanine J-aggregates adsorbed on single silver nanoaggregates by surface-enhanced Raman scattering and emission spectroscopy, *Bull. Chem. Soc. Jpn.* 82 (9) (2009) 1126–1132.
- [33] Y. Kitahama, A. Ogawa, Y. Tanaka, S. Obeidat, T. Itoh, M. Ishikawa, Y. Ozaki, Difference in time dependence of surface-enhanced Raman scattering spectra of thiocarbocyanine J- and H-aggregates adsorbed on single silver nanoaggregates, *Chem. Phys. Lett.* 493 (4–6) (2010) 309–313.
- [34] Y. Kitahama, Y. Tanaka, T. Itoh, Y. Ozaki, Power-law analysis of surface-plasmon-enhanced electromagnetic field dependence of blinking SERS of thiacyanine or thiocarbocyanine adsorbed on single silver nanoaggregates, *Phys. Chem. Chem. Phys.* 13 (2011) 7439–7448.
- [35] C.R. Zamecnik, A. Ahmed, C.M. Walters, R. Gordon, G.C. Walker, Surface-enhanced Raman spectroscopy using lipid encapsulated plasmonic nanoparticles and J-aggregates to create locally enhanced electric fields, *J. Phys. Chem. C* 117 (4) (2013) 1879–1886.
- [36] Y. Kitahama, D. Araki, Y.S. Yamamoto, T. Itoh, Y. Ozaki, Different behaviour of molecules in dark SERS state on colloidal Ag nanoparticles estimated by truncated power law analysis of blinking SERS, *Phys. Chem. Chem. Phys.* 17 (2015) 21204–21210.
- [37] COMSOL MULTIPHYSICS v5.2, COMSOL, Inc.
- [38] A.D. Rakić, A.B. Djurišić, J.M. Elazar, M.L. Majewski, Optical properties of metallic films for vertical-cavity optoelectronic devices, *Appl. Opt.* 37 (22) (1998) 5271–5283.
- [39] C.F. Frontiers, D.R. Huffman, *Absorption and Scattering by an Arbitrary Particle*, Wiley-VCH Verlag GmbH, 2007, pp. 57–81.
- [40] M. Kerker, D.-S. Wang, H. Chew, Surface enhanced Raman scattering (SERS) by molecules adsorbed at spherical particles, *Appl. Opt.* 19 (19) (1980) 3373–3388.
- [41] L.O. Herrmann, V.K. Valev, J. Aizpurua, J.J. Baumberg, Self-sifting of chain plasmons: the complex optics of au nanoparticle clusters, *Opt. Express* 21 (26) (2013) 32377–32385.
- [42] C. Tserkezis, R.W. Taylor, J. Beitner, R. Esteban, J.J. Baumberg, J. Aizpurua, Optical response of metallic nanoparticle heteroaggregates with subnanometric gaps, *Part. Part. Syst. Char.* 31 (1) (2014) 152–160.
- [43] R. Esteban, R.W. Taylor, J.J. Baumberg, J. Aizpurua, How chain plasmons govern the optical response in strongly interacting self-assembled metallic clusters of nanoparticles, *Langmuir* 28 (24) (2012) 8881–8890.
- [44] R.W. Taylor, R. Esteban, S. Mahajan, J. Aizpurua, J.J. Baumberg, Optimizing SERS from gold nanoparticle clusters: addressing the near field by an embedded chain plasmon model, *J. Phys. Chem. C* 120 (19) (2016) 10512–10522.
- [45] N. Harris, M.D. Arnold, M.G. Blaber, M.J. Ford, Plasmonic resonances of closely coupled gold nanosphere chains, *J. Phys. Chem. C* 113 (7) (2009) 2784–2791.
- [46] Y. Ozaki, K. Kneipp, R. Aroca, *Frontiers of Surface-Enhanced Raman Scattering*, John Wiley & Sons Ltd, 2014.
- [47] D.L. Akins, Theory of Raman scattering by aggregated molecules, *J. Phys. Chem.* 90 (8) (1986) 1530–1534.